Mechanical characterization of autoclaved aerated concrete masonry subjected to in-plane loading: Experimental investigation and FE modeling

Mechanical characterization of autoclaved aerated concrete masonry subjected to in-plane loading: experimental investigation and FE modeling

Daniele Ferretti[a] ***, Elena Michelini**[a] **and Gianpaolo Rosati**[b]

[a] *Department of Civil, Environmental, Land Management Engineering and Architecture, University of Parma, P.co Area delle Scienze 181/A, 43124 Parma, Italy, daniele.ferretti@unipr.it, elena.michelini@unipr.it*

[b] *Department of Civil and Environmental Engineering, Politecnico di Milano, Piazza L. da Vinci 32, 20133 Milano, Italy, gianpaolo.rosati@polimi.it*

* Corresponding author. Tel. +39 0521 905943; fax +39 0521 905924.

E-mail address: daniele.ferretti@unipr.it (D. Ferretti).

ABSTRACT

This paper aims to provide a mechanical characterization of autoclaved aerated concrete (AAC) masonry with thin bed joints subjected to in-plane loading. To this purpose, a detailed experimental program has been carried out on masonry beams subjected to bending and masonry panels subjected to uniaxial and biaxial loads. The obtained results have highlighted an almost isotropic behavior of the material. The collected data have been applied to calibrate a well-known numerical macro-model available in the technical literature for the analysis of classical masonry structures. The effectiveness of the proposed procedure has been finally verified by simulating the

experimental behavior of a full-scale AAC bearing wall, through nonlinear finite element analysis.

KEYWORDS

AAC; thin bed masonry; experimental tests; constitutive model; mechanical properties; finite element analysis.

1. INTRODUCTION

In recent years, the increasing demand for flexibility, comfort and energy saving in residential and industrial buildings has led both designers and manufactures to adopt new constructive systems, like Autoclaved Aerated Concrete (AAC) masonry.

AAC is a lightweight cementitious product of calcium silicate hydrates, whose low density is obtained by the presence of air bubbles in the matrix – thanks to the addition of aluminum powder in the mixture during the liquid or plastic phase – to produce a cellular structure [1]. Therefore, it offers excellent sound and thermal insulation properties [2, 3], which have led in the past decades to an increasing use of this material for non-structural applications, especially cladding and infill panels. Anyway, AAC is also characterized by a good mechanical strength and fire-resistance (due to its incombustible nature) that make it suitable for the realization of masonry bearing walls of low-to-medium rise buildings, even in seismic zones [3-10]. Compared with conventional concrete (including concrete made with lightweight aggregates), AAC has typically a lower density (which in turn reduces the seismic inertial forces acting on the structure), ranging from one-sixth to one-third, and by a lower compressive strength, which is almost reduced in the same ratio. The tendency to absorb water, related to the porous structure of the material, can further reduce its structural performances [11]; consequently, specific construction details can be required in order to achieve a satisfactory static behavior.

Since the aforementioned peculiarities make AAC different from conventional masonry materials, it is of fundamental importance to provide a detailed experimental characterization of its mechanical behavior. Test results allow indeed to calibrate sophisticated numerical models to be used in structural analyses, both for the design of

54 new structures and for the assessment/retrofit of existing ones [12].

55 As known, masonry assemblages such as shear walls, infill walls in framed
56 construction or walls supported on beams are generally subjected to a biaxial state of
57 stress, due to the presence of normal stresses parallel and perpendicular to the bed
58 joints, as well as of shear stresses along the joints themselves. Moreover, unreinforced
59 conventional masonry generally exhibits anisotropic properties due to its composite
60 structure, with mortar joints acting as planes of weakness. Therefore, its failure cannot
61 be described solely in terms of the two principal stresses, but a third variable – related to
62 bed joint orientation – must be also considered. For these reasons, several researches in
63 the past focused their attention on the experimental determination of reliable parameters
64 of masonry strength, as well as on the development of failure criteria for masonry
65 elements subjected to in-plane loading (e.g. [13-16]). One of the most complete
66 experimental campaigns relative to masonry subjected to proportional biaxial loading
67 was carried out by Page [17, 18]. These tests were performed on half-scale square
68 panels made of solid clay units to investigate the influence exerted on failure mode and
69 strength by bed joint orientation (with respect to the vertical principal stress direction),
70 as well as by the applied principal stress ratio. Based on these experimental data, biaxial
71 failure surfaces were first derived in terms of the two principal stresses and their
72 orientation to bed joints ([17], [18]) and subsequently in terms of the stress system
73 related to the direction of the joints [19], which is better suited for finite element
74 modeling. Moreover, the same test results were also used in [20] to determine
75 macroscopic elastic and non-linear stress-strain relations. However, it is worth noticing
76 that the strength envelope obtained by Page is of limited applicability for other types of
77 masonry, characterized by different materials, unit shapes and/or geometry. For

78 example, the influence of joint orientation was found to be less significant for grouted
79 concrete masonry, whose experimental behavior under biaxial stresses seems to be
80 essentially isotropic [21]. Further experimental investigations were also carried out on
81 masonry panels subjected to in-plane forces, by considering different unit geometries
82 and materials (concrete blocks, calcium-silicate blocks and clay bricks [22], or grouted
83 unreinforced brick masonry [23]), so as to define suitable failure criteria.
84 It should be also remarked that the results provided from the abovementioned
85 experimental programs could be hardly extended to AAC masonry, also because this
86 latter belongs to "thin bed masonry" typology. The units are indeed connected together
87 through thin glue layers, with thickness usually ranging between 0.5 and 3 mm.
88 Researches carried out on thin bed masonry (among others, e.g. [24-27]) have shown
89 that joint thickness significantly affects masonry behavior. As an example, the
90 compressive strength of thin bed masonry is higher with respect to conventional
91 masonry, since it tends to approach the strength of the blocks. Moreover, its shear and
92 flexural strengths are not significantly affected by the interface bond behavior and
93 therefore thin bed masonry performs more similarly to a continuum under loading,
94 without excessive localization of the failure path along the joints. Biaxial compression
95 tests carried out by Vermeltfoort [28] on thin bed masonry panels with different joint
96 orientations showed that their failure mechanism was characterized by the three
97 following phenomena: spalling of the units with fragments of approximately 20 mm,
98 vertical splitting, and bending of the sample.
99 It is not clear if AAC masonry displays the same behavior. The most of the
100 experimental programs carried out in recent years on this specific type of masonry were
101 indeed mainly focused on the assessment of its seismic performances and were devoted

to the development of seismic design provisions to be included in Design Codes (among others, e.g. [8]-[10], [29]-[31]).

Aim of this research work is to provide a complete description of AAC masonry behavior under in-plane static loading, with particular attention to the softening regime. To the purpose, several experimental tests are performed on both AAC masonry panels and beams, so as to characterize masonry behavior under uniaxial and biaxial compression, flexure and shear, determining not only its elastic parameters and strength values, but also the fracture energies in tension and compression. The collected experimental data can be useful in the calibration of suitable numerical models; as an example, in this work an anisotropic nonlinear constitutive model, well-known in the technical literature for FE analysis of ordinary masonry structures [32-34], is adapted to AAC masonry elements. The so calibrated model is subsequently validated by performing a nonlinear FE analysis on a full-scale AAC masonry wall subjected to a pushover test [31].

2. EXPERIMENTAL PROGRAM ON AAC MASONRY ELEMENTS

The performed experimental program consisted in 33 tests on AAC masonry elements with thin bed joints. A general view of some of the assembled specimens before testing is shown in Figure 1.

In order to characterize the material behavior in compression, several monotonic uniaxial and biaxial tests were performed on small-scale masonry panels, by varying the bed joint orientation with respect to the horizontal axis. Some of the uniaxial tests were carried out under displacement control to obtain the complete stress-strain curve and the

corresponding fracture energy in compression.

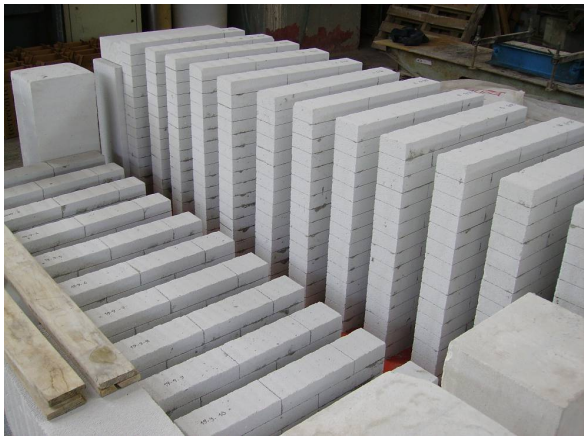

Figure 1. *General view of some of the AAC masonry specimens tested during the experimental program.*

Due to the limited features of the universal testing machines at our disposal, tensile behavior of AAC masonry was instead investigated indirectly, by performing three-point bending tests on small-scale masonry beams. In this case, only two angles of inclination between the bed joints and the horizontal axis were considered (namely 0° and 90°). For each examined typology, two beams were provided of a central notch to guide crack formation and were tested under crack mouth opening displacement (CMOD) control, so obtaining the complete load-deflection response and the corresponding fracture energy in tension. Finally, two small masonry panels were subjected to diagonal compression tests.

2.1 Description of test specimens

All the specimens were prepared by using masonry-type AAC units directly provided by the Manufacturer. It is worth noticing that AAC units are commonly produced in different sizes that may reach 625×250×200 mm; in this last case, masonry panels including a representative number of head and bed joints would be huge and some problems may arise to test them into the frame of a universal testing machine.

143 However, considering that the dimensions of the units available on the market are
144 variable, in the present work it has been preferred to employ non-standard small size
145 bricks, with nominal dimensions equal to 250×50×100 mm. In this way, it has been
146 possible to keep the specimen size small, while having at the same time an adequate
147 number of head and bed joints, so emphasizing their influence on masonry global
148 behavior and increasing possible anisotropic effects. Therefore, the behavior of
149 structural elements realized with larger units and a more limited number of joints should
150 lie between the two "limit cases" of homogeneous material (previously investigated by
151 the same Authors in [35]) and the here investigated masonry formed by small units. In
152 any case, experimental evidences have shown that the use of scaled bricks does not
153 seem to alter substantially the results, as will be discussed in more details in the
154 forthcoming Sections.
155 A deep characterization of the raw autoclaved aerated concrete adopted for the
156 realization of units can be found in [35]. Its main mechanical characteristics were:
157 average density ρ_b = 550 kg/m^3, average compressive strength f_b = 3.1 MPa (as
158 determined on cubes with an edge length of 100 mm), average modulus of rupture
159 $f_{t,b}$ = 0.6 MPa, and elastic modulus E_b = 1320 MPa.
160 Units were assembled by using a specific cementitious grey glue produced by the
161 same Manufacturer, mainly composed of Portland cement, silica sand and specific
162 additives, with a water dosage equal to 24% in weight. This grey glue was a guaranteed
163 performance mortar characterized by the following main properties: average density
164 ρ_g = 1300 kg/m^3, average compressive strength of cylindrical specimens f_g = 7 MPa (it
165 was instead equal to 6 MPa when determined on 40×40×160 mm prisms), average
166 modulus of rupture $f_{t,g}$ = 2.7 MPa, elastic modulus E_g = 5300 MPa. The nominal

167 thickness of head and bed joints was equal to 1.5 mm.

168 To allow a complete drying of the glue and the reaching of stationary moisture
169 conditions, all the specimens were stored in laboratory for more than three months. At
170 time of test execution, all samples were characterized by an average moisture content
171 approximately equal to 2.4% and by an average density ρ = 550 kg/m^3.

172 As already mentioned, uniaxial and biaxial compression tests were performed on
173 23 small-scale masonry panels, with length of 625 mm, thickness equal to 100 mm and
174 height equal to 750 mm. Two additional uniaxial tests were performed on smaller
175 square panels with an edge length of 250 mm, characterized by the same thickness. This
176 last specimen geometry was also adopted for the two diagonal compression tests.
177 Flexural tests were instead carried out on six small-scale masonry beams with length of
178 625 mm, thickness equal to 100 mm and height equal to 250 mm. Further details about
179 sample characteristics and adopted test arrangements are reported in the following
180 Sections.

181 ***2.2 Characterization of AAC masonry panels in compression***

182 ***2.2.1 Uniaxial compression tests***

183 Uniaxial compression tests were performed on 17 small-scale masonry panels
184 (Figure 2a). In order to study the influence exerted by the geometrical arrangement of
185 units and joints on masonry compressive strength, 5 specimen typologies, characterized
186 by a different inclination θ of glue beds – equal to 0°, 22°, 45°, 68° and 90° with respect
187 to the horizontal direction – were considered, as depicted in Figure 2a. The same Figure
188 also provides specimen nominal dimensions, as well as their denomination, which is
189 composed by the acronym PMC (which stands for Panel Masonry Compression),

followed by two digits, the first one representing the angle of inclination of glue beds and the second one (in brackets) the total number of tested samples belonging to a considered typology.

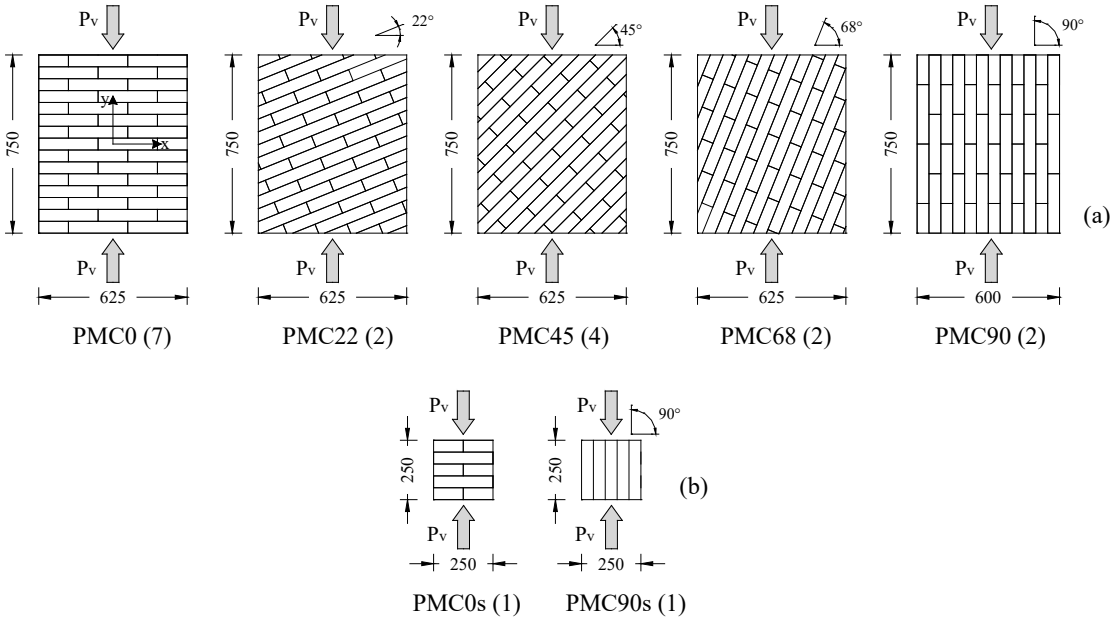

Figure 2. *Sketch of uniaxial compression tests on masonry panels (a) PMC and (b) PMCs (characterized by reduced dimensions).*

A larger part of this experimental program (15 samples) was carried out at the Laboratory of the AAC Manufacturer Company, by using a Metrocom PV50 press working under loading control, with a capacity of the hydraulic actuator equal to 5000 kN [36]. The adopted test arrangement is shown in Figure 3; in order to apply a distributed load, a 650 mm long steel rigid beam with I-section was placed on the top of the sample. Panel surfaces were preliminary flattened by sandpaper to eliminate any irregularity and thereby ensure a complete contact between the specimen itself and the testing apparatus. Furthermore, two overlapping Teflon sheets were interposed to minimize the confinement effect due to friction and apply a uniform state of stress. The most of these tests simply provided the uniaxial compressive strengths f_{mx}, f_{my} in the two

masonry principal directions (respectively parallel, x, and perpendicular, y, to glue beds). Three of these 15 samples – denoted as PMC0-2, PMC0-3, and PMC90-1 – were also instrumented with 6 linear variable displacement transducers (LVDTs) aligned along x and y directions on the two opposite panel faces, as shown in Figure 3b. The LVDTs were installed to measure vertical and horizontal strains (ε_v and ε_h), so allowing the evaluation of the elastic moduli E_x and E_y in the two masonry principal directions, as well as the Poisson coefficient ν. Moreover, it was also possible to follow the initial part of the softening branch by performing a gradual unloading of the specimen after the reaching of the peak load.

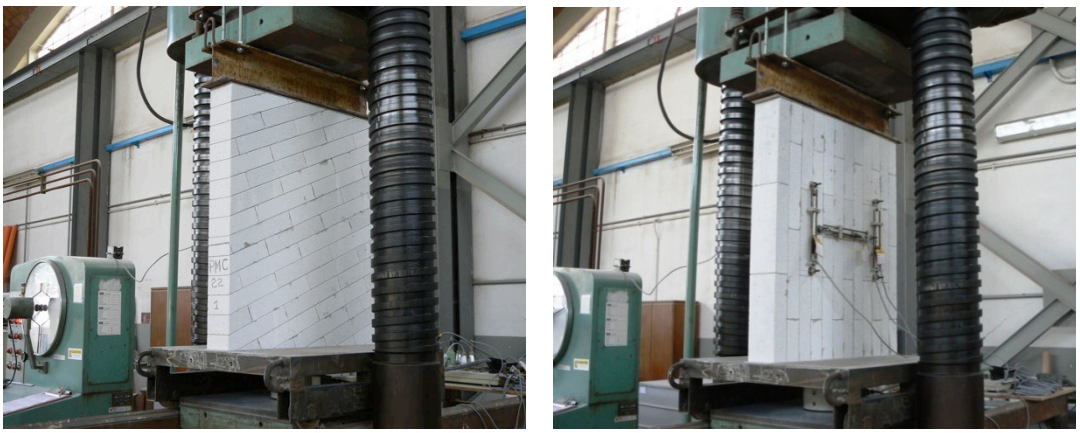

(a) (b)

Figure 3. *General setup of uniaxial compression tests performed under loading control: (a) not instrumented and (b) instrumented small-scale masonry panels (PMC).*

The remaining two samples (respectively indicated as PMC0-7 and PMC90-2 according to Figure 2a) were tested at the Materials and Structures Laboratory of Milan Polytechnic University, by using a 1000 kN Schenck press working under displacement control (Figure 4a). Two 650 mm long steel rigid beams with I-section were placed on the top and bottom bases of the specimen, by interposing two thin Teflon sheets in order to reduce friction. All samples were instrumented with 6 LVDTs aligned along x and y

directions on the two opposite panel faces, as shown in Figure 4a. These tests provided the complete stress-strain curve for the material in compression.

The so obtained results were subsequently integrated by testing two additional smaller panels (Figure 2b), respectively characterized by horizontal (PMCs0) and vertical (PMCs90) glue beds.

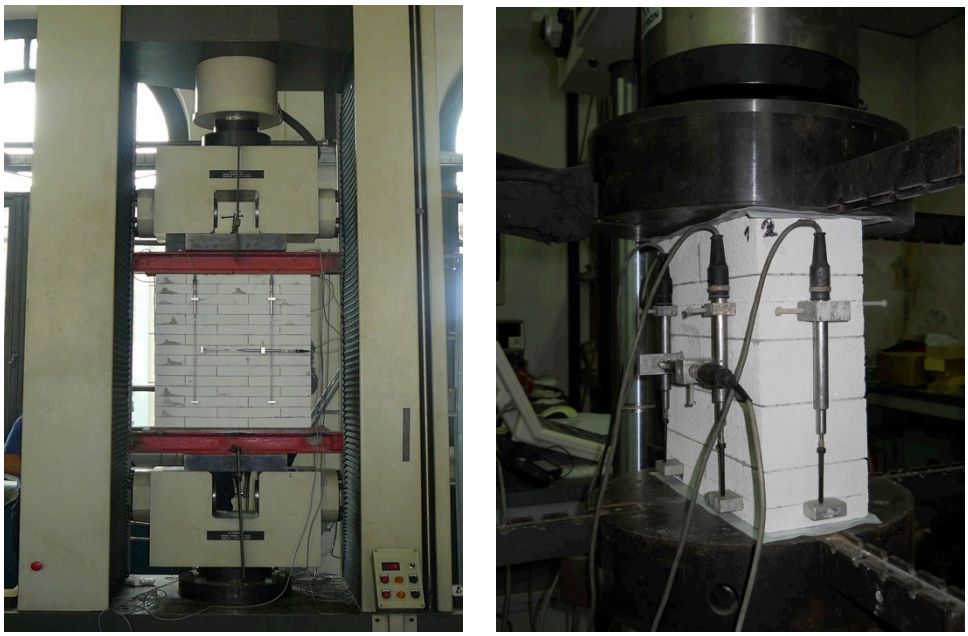

(a) (b)

Figure 4. *General setup of uniaxial compression tests performed under displacement control: (a) small-scale masonry panels (PMC) and (b) square specimens with reduced dimensions (PMCs).*

In this last case, a 100 kN Instron 8862 press working under displacement control was used and the samples were still instrumented with 6 LVDTs aligned along x and y directions on the two opposite panel faces, with two further vertical LVDTs in the thickness (Figure 4b). These two additional specimens were realized in order to achieve a better description of the post-peak response, since bigger panels displayed local failures that determined in some cases sudden jumps in the softening branch of the stress-strain curve.

The main results of the above-described tests are summarized in Table 1 in terms

of experimental failure load $P_{v,u}$ and corresponding vertical compressive stress σ_v for each tested panel.

Sample	#	Test control	L (mm)	t (mm)	H (mm)	$P_{v,u}$ (kN)	σ_v (MPa)	σ_x (MPa)	σ_y (MPa)	τ_{xy} (MPa)
PMC0	1	LC	622.00	100.90	740.00	160.82	-2.56	0.00	-2.56	0.00
PMC0	2	LC	621.00	99.50	746.00	151.27	-2.45	0.00	-2.45	0.00
PMC0	3	LC	621.00	99.11	745.00	167.50	-2.72	0.00	-2.72	0.00
PMC0	4	LC	622.00	99.86	744.00	140.75	-2.27	0.00	-2.27	0.00
PMC0	5	LC	623.00	99.71	745.00	171.33	-2.76	0.00	-2.76	0.00
PMC0	6	LC	623.00	99.87	747.00	151.27	-2.43	0.00	-2.43	0.00
PMC0	7	DC	623.00	100.00	756.00	172.86	-2.77	0.00	-2.77	0.00
PMCs0	1	DC	240.00	100.00	250.00	67.14	-2.80	0.00	-2.80	0.00
PMC90	1	LC	610.00	100.00	741.00	156.00	-2.56	-2.56	0.00	0.00
PMC90	2	DC	610.00	100.00	740.00	143.57	-2.35	-2.35	0.00	0.00
PMCs90	1	DC	250.00	100.00	246.00	72.03	-2.88	-2.88	0.00	0.00
PMC22	1	LC	627.00	100.00	751.00	141.84	-2.26	-0.32	-1.94	0.79
PMC22	2	LC	625.00	100.00	749.00	143.59	-2.30	-0.32	-1.98	0.80
PMC45	1	LC	627.00	100.00	747.00	133.08	-2.12	-1.06	-1.06	1.06
PMC45	2	LC	625.00	100.00	748.00	137.46	-2.20	-1.10	-1.10	1.10
PMC45	3	LC	623.00	99.50	749.00	139.21	-2.25	-1.12	-1.12	1.12
PMC45	4	LC	625.00	100.00	748.00	139.21	-2.23	-1.11	-1.11	1.11
PMC68	1	LC	624.00	100.00	748.00	134.83	-2.16	-1.86	-0.30	0.75
PMC68	2	LC	625.00	100.00	748.00	128.70	-2.06	-1.77	-0.29	0.72

LC = loading control
DC = displacement control

Table 1. *Uniaxial compression tests on AAC masonry panels (PMC and PMCs): effective dimensions of the specimens and experimental failure loads.*

The same Table also reports the total stress state related to bed joints σ_x, σ_y and τ_{xy} (being *x, y* the directions respectively parallel and perpendicular to bed joints, as depicted in Figure 2a), which has been subsequently deduced by using the following standard relations [19]:

$$\sigma_x = \frac{\sigma_v + \sigma_h}{2} - \frac{\sigma_v - \sigma_h}{2}\cos(2\theta)$$

$$\sigma_y = \frac{\sigma_v + \sigma_h}{2} + \frac{\sigma_v - \sigma_h}{2}\cos(2\theta) \qquad (1)$$

$$\tau_{xy} = \frac{\sigma_v - \sigma_h}{2}\sin(2\theta)\,.$$

These equations, that are valid for a general biaxial state of stress (being σ_v and σ_h the

256 vertical and horizontal principal stresses, respectively, and θ the angle between bed
257 joints and the horizontal axis), have been here applied to the uniaxial case by simply
258 posing $\sigma_h = 0$. Table 1 also indicates the effective specimen dimensions (L, t, H), as
259 well as the adopted type of testing, that is to say under displacement or loading control
260 (respectively indicated as DC and LC).

261 Experimental results highlighted that the compressive strengths in the two
262 principal directions x-y – respectively obtained as the average peak stress values σ_v for
263 PMC90 and PMC0 samples – were almost equal to each other ($f_{mx} \approx f_{my} \approx 2.60$ MPa). A
264 slight reduction of masonry compressive strength - ranging between 13 and 24% - was
265 instead observed for other angles of bed joints (that is $\theta = 22°, 45°, 68°$).

266 Based on the results of this investigation, it seems that bed joint orientation exerts
267 only a limited influence on the compressive behavior of tested panels, as also reported
268 in the literature for other types of thin bed masonry [25]. This is mainly due to the
269 isotropic behavior of AAC units (which do not have internal perforations), as well as to
270 the presence of thin glue joints with a relatively high strength.

271 Moreover, AAC masonry compressive strength in the two principal directions x-y
272 appears to be only slightly lower with respect to that of the raw material, as determined
273 on AAC prisms and cubes sawed from some of the tested masonry specimens (Figure
274 5a). The first ones, characterized by a 40 mm square basis and 80 mm height, provided
275 indeed an average uniaxial compressive strength approximately equal to $f_{AAC} = 2.8$ MPa,
276 while for 40 mm side cubes a value of $f_{AAC,cube} = 3.1$ MPa was found. These values were
277 almost coincident with those provided from standard tests previously carried out on the
278 adopted raw material (see [35] for further details), as well as with those available in the
279 technical literature for a material with similar density and moisture content [5-6].

Anyway, it should be kept in mind that AAC compressive strength depends on the geometry and dimensions of tested blocks. Compression tests performed on raw-AAC panels with nominal dimensions equal to those of masonry ones (625 x 750 x 100 mm, Figure 5b) and produced by the same Manufacturer provided indeed an average compressive strength f_c = 2.4 MPa, which is comparable to that obtained from masonry specimens.

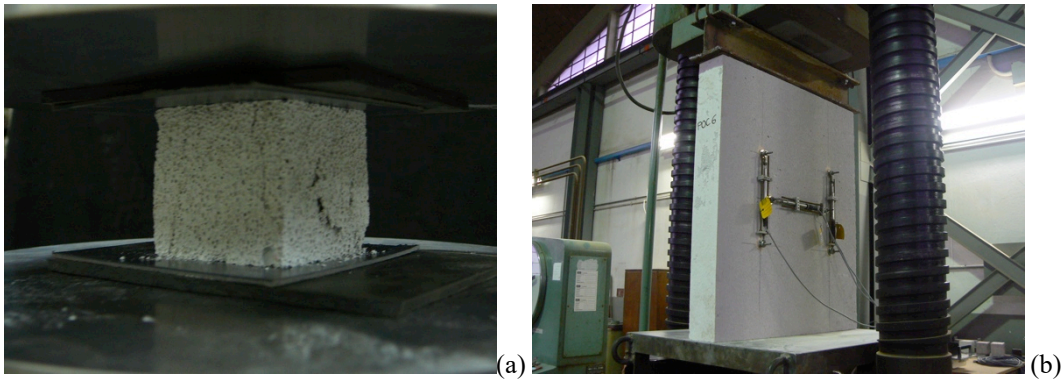

(a) (b)

Figure 5. *Uniaxial compression tests on homogeneous AAC samples: (a) cubes with an edge length of 40 mm and (b) panels with the same geometry and dimensions of PMC masonry ones.*

This result is not surprising when considering both the high strength of the cementitious glue and the relatively small size of adopted units, which allowed a random redistribution of the defects in the tested panel. In homogeneous samples, failure was instead mainly localized near the weaker edge, related to the expansion process. Moreover, at time of test execution, masonry samples were characterized by a slightly lower moisture content with respect to homogeneous ones ([35]).

Masonry elastic properties are summarized in Table 2. Elastic moduli were determined as the chord slope of the stress - vertical strain curve (within a stress interval ranging from 0.05 σ_v and 0.33 σ_v), so obtaining an average value respectively equal to E_x = 1700 MPa for PMC90 samples (with vertical glue beds) and E_y = 1400 MPa for

PMC0 samples (with horizontal glue beds). This last value was calculated by discarding the result relative to PMCs0 sample, which was characterized by an anomalous more rigid behavior compared to the other ones belonging to the same typology. The obtained values are of the same order of magnitude as the ones provided by Manufacturer certifications and technical sheets, which range between 1400 MPa and 1750 MPa (referred to a masonry with horizontal glue beds). Poisson coefficient was instead evaluated as the ratio between horizontal and vertical strains (ε_h / ε_v), obtaining an average value almost equal to $\nu \cong 0.30$ in both the two main directions. It can be observed that the so determined elastic properties are similar, even if not identical, to those previously derived on homogeneous panels, which were respectively equal to E = 1352 MPa and ν = 0.38, as reported in [35].

Table 2 also summarizes the strains values corresponding to peak stresses, which were respectively equal, on average, to ε_{px} = 1.8‰ and ε_{py} = 2.2‰.

Sample	**#**	**Test control**	**E_x (MPa)**	**E_y (MPa)**	**ν (MPa)**	**ε_{px} (‰)**	**ε_{py} (‰)**
PMC0	2	LC		1417	0.32		2.00
PMC0	3	LC		1392	0.38		2.20
PMC0	7	DC		1346	0.29		2.40
PMCs0	1	DC		1737	0.35		1.68
PMC90	1	LC	1653		0.29	1.90	
PMC90	2	DC	1713		0.26	1.50	
PMCs90	1	DC	1719		0.25	2.10	

LC = loading control
DC = displacement control

Table 2. *Uniaxial compression tests on AAC masonry panels (PMC and PMCs): elastic moduli E_x, E_y, Poisson ratio ν and compressive peak strains ε_{px} and ε_{py}.*

Finally, the observed crack patterns at failure are shown in Figure 6. Depending on the orientation of the bed joints to the applied load, failure mainly occurred by cracking and sliding in the bed and/or head joints, or in a combined mechanisms

involving cracking in both units and joints. As can be seen from Figure 6a-b, for both PMC0 and PMC22 panels a major crack developed in the direction perpendicular to bed joints, alternatively crossing AAC blocks and thin glue layers. On the contrary, in PMC90 and PMC68 samples (Figure 6d-e), cracks mainly developed along glue beds, while for PMC45 ones (Figure 6c) the observed failure mode was less defined, with diagonal cracks spreading at the same time both in glue beds and AAC blocks.

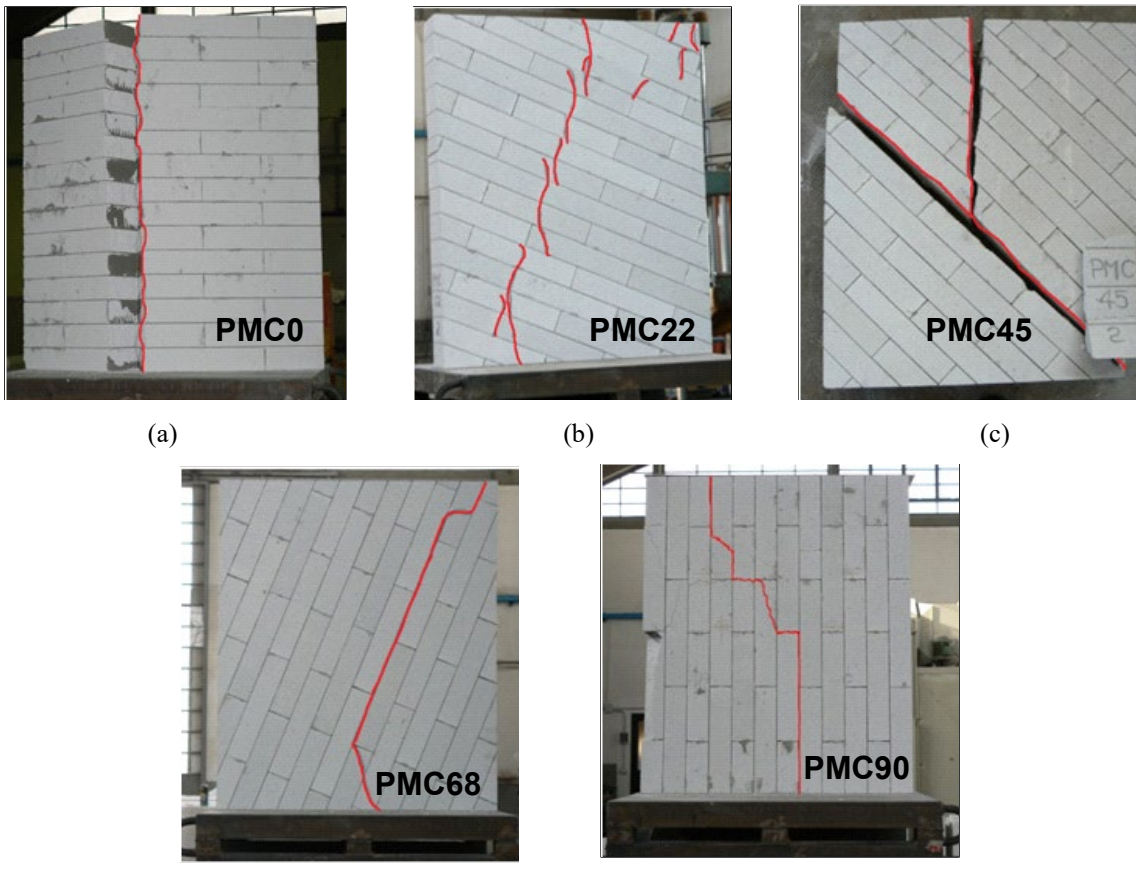

Figure 6. *Uniaxial compression tests on AAC masonry panels (PMC): observed crack patterns at failure as function of bed joint inclination.*

2.2.2 Biaxial compression tests

Biaxial compression tests were carried out on the same panel typologies already

subjected to uniaxial compression, as depicted in Figure 7a. As can be seen from the same Figure, these panels were named PMB (which stands for Panel Masonry Biaxial compression), followed by two digits, the first one representing the angle of inclination of glue beds with respect to the horizontal axis and the second one (in brackets) the total number of tested samples belonging to a considered typology. In this case, three different inclinations of bed joints were considered (0°, 22°, and 45°) for a total of 6 samples, two for each typology. Since equal compressive forces were applied in the two principal directions, 68° and 90° inclinations were indeed coincident with 22° and 0°.

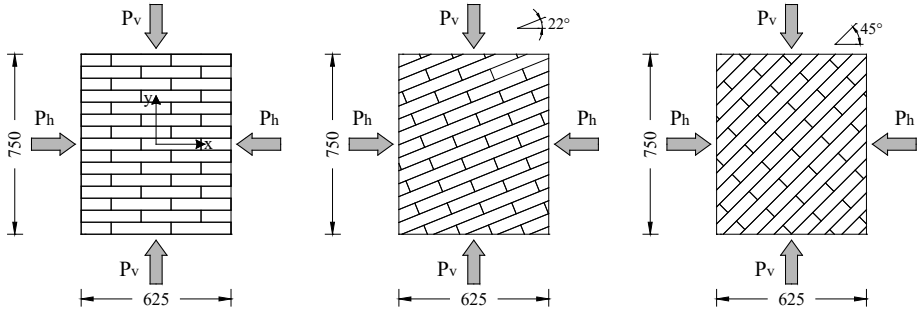

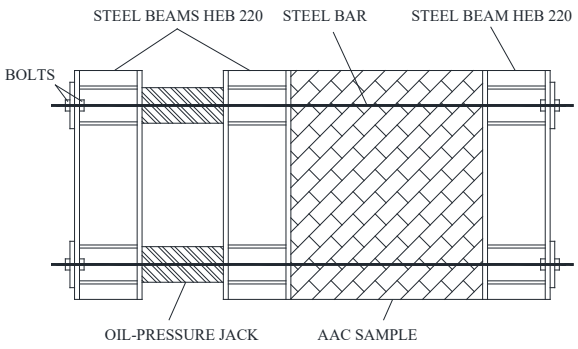

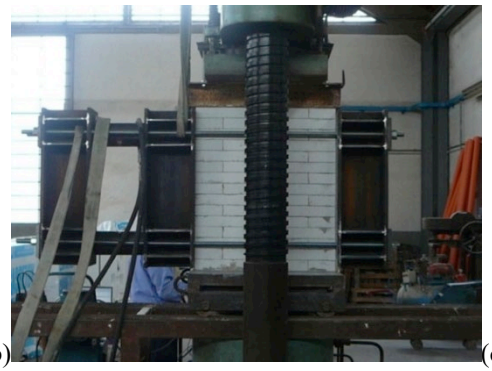

Figure 7. *(a) Sketch of biaxial compression tests on masonry panels (PMB); (b) sketch and (c) general view of the adopted setup.*

Vertical load P_v was applied by using the same Metrocom PV50 press already used for uniaxial compression tests, by adopting a similar loading arrangement (with a steel rigid beam on the top of the sample and thin Teflon layers interposed between the

sample and the loading apparatus). Lateral confinement P_h was instead applied by adopting the device depicted in Figure 7b-c, formed by a system of steel rigid beams connected together through steel ribbed bars. These beams were placed on the sides of the AAC sample (by interposing the usual thin Teflon layers) and were used as contrast for two oil-pressure jacks, aligned in the horizontal direction. Biaxial tests were performed under loading control by monitoring that the same value of vertical and horizontal pressure was simultaneously applied on sample surfaces (the two loading devices were indeed not directly connected to each other). In this case, none of the specimen was instrumented.

The main results of the above described tests are summarized in Table 3, in terms of experimental failure loads $P_{v,u}$ and $P_{h,u}$, as well as corresponding stresses σ_v and σ_h. From these values, the total stress state related to bed joints σ_x, σ_y and τ_{xy} has been also determined (being *x, y* the directions respectively parallel and perpendicular to bed joints, as depicted in Figure 7a), by still applying Equations 1. The obtained results confirm that the bed joint angle exerts only a limited influence on the strength of masonry; moreover, the biaxial strength value is substantially comparable with the uniaxial one. Table 3 also reports the effective specimen dimensions (*L*, *t*, *H*).

Sample	#	Test control	L (mm)	t (mm)	H (mm)	$P_{v,u}$ (kN)	σ_v (MPa)	$P_{h,u}$ (kN)	σ_h (MPa)	σ_x (MPa)	σ_y (MPa)	τ_{xy} (MPa)
PMB0	1	LC	624	100	761	138.09	-2.21	165.52	-2.18	-2.18	-2.21	0.00
PMB0	2	LC	623	100	760	143.10	-2.30	171.61	-2.26	-2.26	-2.30	0.00
PMB22	1	LC	626	100	749	137.66	-2.20	159.54	-2.13	-2.14	-2.19	0.02
PMB22	2	LC	625	100	750	146.19	-2.34	173.48	-2.31	-2.32	-2.34	0.01
PMB45	1	LC	626	100	748	124.51	-1.99	142.12	-1.90	-1.95	-1.95	0.04
PMB45	2	LC	624	100	748	137.22	-2.20	161.57	-2.16	-2.18	-2.18	0.02

LC = loading control
DC = displacement control

Table 3. *Biaxial compression tests on AAC masonry panels (PMB): effective dimensions of the specimens and experimental failure loads.*

366 The observed crack patterns at failure are depicted in Figure 8. As can be seen, all
367 panels showed the same failure mode, characterized by an out-of-plane expansion in the
368 unconfined direction, regardless of bed joint orientation. Spalling of small masonry
369 fragments was also observed.

370 (a) (b) (c)

371 ***Figure 8.*** *Biaxial compression tests on AAC masonry panels (PMB): observed crack patterns at failure as*
372 *function of bed joint inclination.*

373 ***2.3 Characterization of AAC masonry beams in flexure***

374 Three-point bending tests were performed on six AAC small-scale masonry
375 beams, with nominal dimensions equal to 625 x 250 x 100 mm (Figure 9).

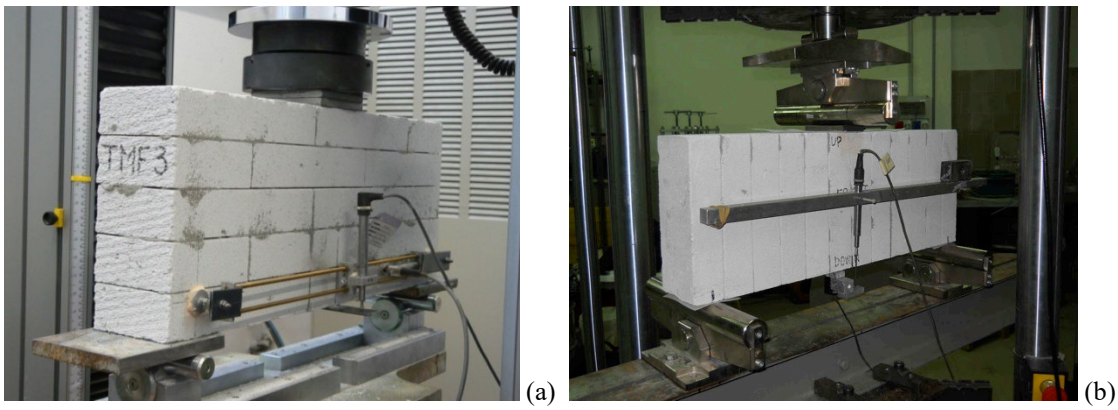

376 (a) (b)

377 ***Figure 9.*** *Three-point bending tests on AAC masonry beams BMF (a) without and (b) with notch:*
378 *adopted setup.*

379 The main characteristics of the tested samples, as well as the adopted
380 nomenclature are summarized in Figure 10. In this case, the acronym BMF (which
381 stands for Beam Masonry Flexure) has been adopted, followed by a number
382 representing the angle of inclination of bed joints with respect to the horizontal axis; a
383 further digit (in brackets) indicates the number of tested specimens belonging to the
384 same typology. In more detail, 4 specimens BMF0 (with horizontal bed joints) and 2
385 specimens BMF90 (with vertical bed joints) were realized; for each typology, 2 beams
386 were provided of a central notch, so as to guide crack formation. It should be here
387 observed that the two BMF90 specimens were characterized by different effective
388 lengths and net spans, as highlighted in Table 4. The first sample was indeed formed by
389 an odd number of units (13), so having the notch placed at half-width of the central
390 brick line; however, the experimental failure was localized in correspondence of one of
391 the adjacent glue joints. For this reason, the other specimen was realized with an even
392 number of units (one less than sample BMF90-1), to place the notch exactly in
393 correspondence of the glue joint.

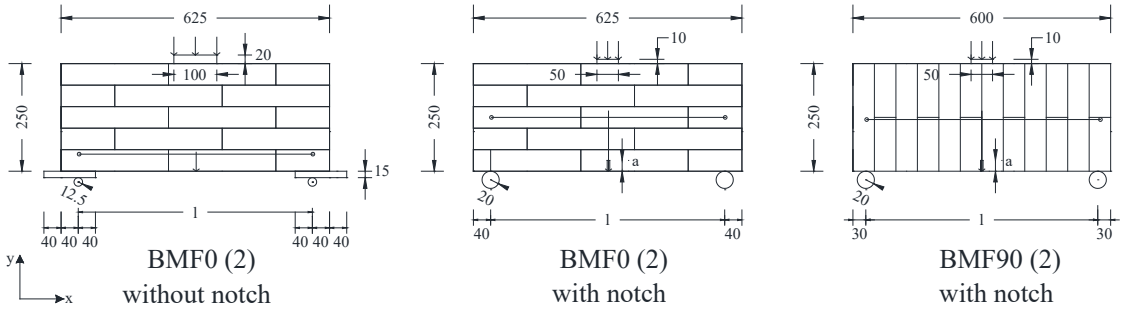

394

395 ***Figure 10.*** *Sketch of three-point bending tests on AAC masonry beams BMF: (a) unnotched specimens*
396 *BMF0; specimens (b) BMF0 and (c) BMF90 with a central notch.*

397 The two unnotched specimens were tested at the Laboratory of the AAC
398 Manufacturer Company, by using an Instron 5882 press working under loading control,

399 with a loading rate of about 1 kN/min (Figure 9a). The 4 notched samples were instead
400 tested at the Materials and Structures Laboratory of Milan Polytechnic University, by
401 using an Instron 8862 press working under CMOD control, with a loading rate of
402 1 μm/min (Figure 9b). All the specimens were instrumented with a LVDT properly
403 fixed on a bar installed over the two supports, in order to monitor the true midspan
404 deflection during test execution (Figure 9 a-b).

405 The performed tests provided the failure load in flexure $P_{u,fl}$ for the two
406 investigated bed joint angles, as reported in Table 4.

Sample	#	Test control	L (mm)	t (mm)	H (mm)	a (mm)	l (mm)	$P_{u,fl}$ (kN)	f'_{tx} (MPa)	G_{fx} (N/mm)	f'_{ty} (MPa)	G_{fy} (N/mm)
BMF0	1	LC	625.4	100.6	251.2	0.0	545.4	2.67	0.34	-		-
BMF0	2	LC	624.2	100.1	251.7	0.0	544.2	2.94	0.38	-		-
BMF0	3	DC	625.0	100.0	250.0	37.5	545.0	2.34	0.42	6.4E-03		-
BMF0	4	DC	626.0	100.0	258.0	25.0	546.0	2.27	0.34	7.8E-03		-
BMF90	1	DC	660.0	100.0	250.0	12.5	600.0	2.56		-	0.37	4.5E-03
BMF90	2	DC	610.0	100.0	240.0	24.0	550.0	1.31		-	0.23	5.8E-03

407 LC = loading control
408 DC = displacement control

409 ***Table 4.*** *Three-point bending tests on AAC masonry beams (BMF): effective dimensions of the specimens,*
410 *experimental failure loads, indirect tensile strengths and fracture energies in tension.*

411 The corresponding flexural tensile strengths (moduli of rupture) in the two
412 examined directions were subsequently determined through a liner elastic FE inverse
413 analysis, so obtaining an average value respectively equal to f'_{tx} = 0.37 MPa and
414 f'_{ty} = 0.30 MPa. Moreover, tests carried out under CMOD control allowed the
415 determination of the complete post-peak load-deflection response and consequently of
416 the two average fracture energies in tension, respectively equal to $G_{fx} = 7.10 \cdot 10^{-3}$ N/mm
417 and $G_{fy} = 5.15 \cdot 10^{-3}$ N/mm. The obtained results, as well as the effective sample
418 dimensions, are reported in detail in Table 4. As can be seen, the first BMF90 sample
419 provided a tensile strength comparable to that obtained for BMF0 samples, while the

second one presented a value approximately 40% lower, probably due to a not proper filling of the central glue joint.

It can be also observed that both the strength and the fracture energy of masonry samples in the two examined directions are comparable to those of the homogeneous material, as reported in the technical literature [5, 35, 37, 38].

2.4 Characterization of AAC masonry panels in diagonal compression

The characterization of AAC masonry behavior was completed through the testing of two small panels in diagonal compression, as depicted in Figure 11a-b. Those samples, named PMS (Panel Masonry Shear), were characterized by nominal dimensions equal to 250 x 250 x100 mm. The tests were still carried out at the Materials and Structures Laboratory of Milan Polytechnic University, by using an Instron 8862 press to apply the vertical load P_v. In order to avoid the crushing of loaded angles and to obtain a uniform state of stress, thin cardboard layers were interposed between the loading platens and the sample, as shown in Figure 11b.

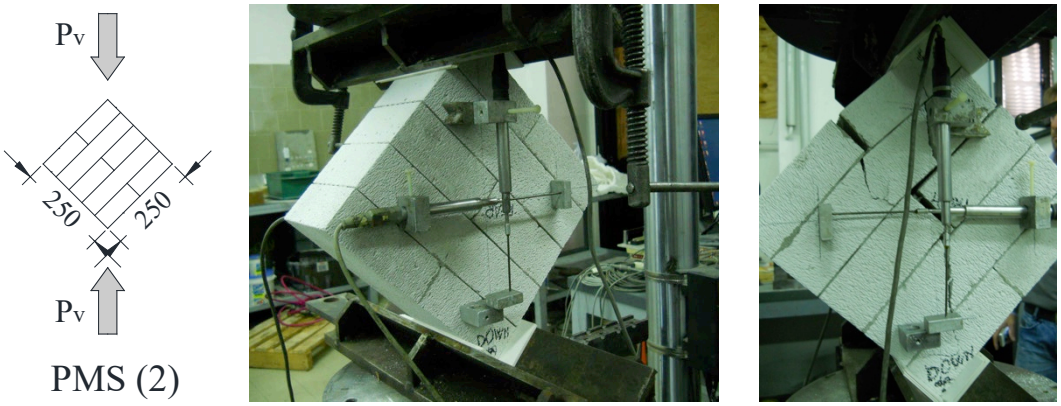

(a) (b) (c)

Figure 11. *(a) Sketch and (b) adopted arrangement of diagonal compression tests on small AAC masonry panels PMS; (c) observed failure mode.*

As can be seen from the same Figure, each sample was instrumented with 2

vertical and 2 horizontal LVDTs, so as to record panel strains with increasing loads.

The obtained results, as well as the effective sample dimensions, are summarized in Table 5, in terms of vertical load at failure P_v and corresponding masonry shear strength (under zero compressive stresses) $f_{v0} = 0.7P_v / A_n$, being A_n the net area of the panel. The latter has been evaluated as $A_n = t\,(H+L)/2$, where H and L are the sides of the panel and t is the thickness. As can be observed from Table 5, these values are rather high if compared to those suggested in technical Codes (e.g., [39]) or determinable with common empirical relations, such as $f_{v0} \approx 0.15\, f_m$, being f_m the masonry compressive strength [40].

Sample	#	Test control	L (mm)	t (mm)	H (mm)	P_v (kN)	f_{v0} (MPa)	σ_x (MPa)	σ_y (MPa)	τ_{xy} (MPa)
PMS	1	DC	240	100	240	19.91	0.59	-0.49	-0.49	0.92
PMS	2	DC	250	100	250	25.74	0.73	-0.60	-0.60	1.14

LC = loading control
DC = displacement control

Table 5. *Diagonal compression tests on small AAC masonry panels (PMS): effective dimensions of the specimens and experimental failure loads.*

The same Table also reports the total stress state related to bed joints σ_x, σ_y and τ_{xy}. As concerns the observed failure modes, both the specimen presented the spreading of a main sub-vertical crack, alternatively crossing AAC blocks and glue joints (Figure 11c).

3. CALIBRATION OF A NUMERICAL MACRO-MODEL FOR AAC MASONRY BASED ON THE EXPERIMENTAL RESULTS

The described experimental results have been used for the calibration of the well-known macro-model proposed by Lourenço et al. [32-34] for the analysis of masonry structures. This model, which treats masonry as an anisotropic continuum and describes

its behavior in terms of average stresses and strains, seems an appropriate tool for simulating the behavior of AAC walls, as well as that of other types of thin bed masonry [25], due to the quite limited influence of the interface. For finite element analyses, the material model has been implemented in [41] into a computer algorithm that handles plasticity features like return mapping, corners, apex, etc. This algorithm has been here converted into a user material subroutine (UMAT) and implemented into the general purpose finite element code ABAQUS [42] to perform numerical simulations.

In the following Sections, the adopted model will be first briefly described and its calibration to the case of AAC masonry will be subsequently discussed.

3.1 Main features of the adopted macro-model

The considered model [32-34], which has been developed with reference to general plane stress conditions, represents an extension of conventional formulations for isotropic quasi-brittle materials to describe orthotropic behavior. Two different failure criteria are adopted for tension and compression, respectively "Rankine-type" and "Hill-type", whose equations [33] are recalled in Figure 12a. As can be seen in Figure 12b, the non-linear behavior of masonry in compression $\overline{\sigma}_{ci} - \kappa_c$ (where the subscript *i* refers to the material axis *x* or *y*) is described through a parabolic plastic stress-strain relationship ($\overline{\sigma}_{ai} - \kappa_c$, according to Fig. 12b) until the reaching of the peak value, which is usually different in the two principal orthotropic directions *x*-*y* - namely $\overline{\sigma}_{px} = f_{mx}$ and $\overline{\sigma}_{py} = f_{my}$. After the peak, a parabolic/exponential softening branch ($\overline{\sigma}_{bi} - \kappa_c$ and $\overline{\sigma}_{di} - \kappa_c$, respectively) is adopted in both directions, characterized by different fracture energies G_{fcx} and G_{fcy}. The inelastic work $g_{fci} = G_{fci}/h$ in Figure 12 is

484 related to the fracture energy G_{fci} through the equivalent length h, which corresponds to
485 a representative dimension of the mesh size (so that the obtained results are objective
486 with regard to mesh refinement). According to [32], the compressive law shown in
487 Figure 12b can be defined on the basis of three stresses (that is initial, mean and residual
488 ones), which are determined as a fraction of the peak value $\bar{\sigma}_{pi} = f_{mi}$ through the
489 following relations: $\bar{\sigma}_{ii} = 1/3\ f_{mi}$, $\bar{\sigma}_{mi} = 1/2\ f_{mi}$, $\bar{\sigma}_{ri} = 1/10\ f_{mi}$. The equivalent plastic
490 strain κ_p, corresponding to the peak compressive strength, is assumed to be an
491 additional material parameter. Furthermore, in order to obtain a mesh independent
492 energy dissipation, it should be posed [32]:

493 $$\kappa_{mi} = \frac{75}{67}\frac{G_{fci}}{h\ f_{mi}} + \kappa_p, \qquad (2)$$

494 with the limitations reported in [32, 34].

495 The nonlinear behavior of masonry in tension is instead described through an
496 exponential softening plastic stress-strain relationship $\bar{\sigma}_{ti} - \kappa_t$, with different tensile
497 strengths (f_{tx} and f_{ty}) and fracture energies (G_{fx} and G_{fy}) in the two principal orthotropic
498 directions (Figure 12c). The exhaustive theoretical formulation of the adopted model
499 can be found in [32-34], to which reference is made for further details.
500 To be correctly calibrated, the considered model requires the knowledge of seven
501 parameters governing material strength (respectively indicated as $f_{tx}, f_{ty}, f_{mx}, f_{my}$, α, β and
502 γ), as well as five inelastic parameters governing the plastic stress-strain relationships
503 (G_{fx}, G_{fy}, G_{fcx}, G_{fcy} and κ_p). The first four strength properties (which represent uniaxial
504 tensile f_{ti} and compressive f_{mi} strengths along the material axes $i = x, y$) can be
505 determined by performing uniaxial tension and compression tests on masonry

specimens, along the two main directions respectively parallel and perpendicular to mortar beds.

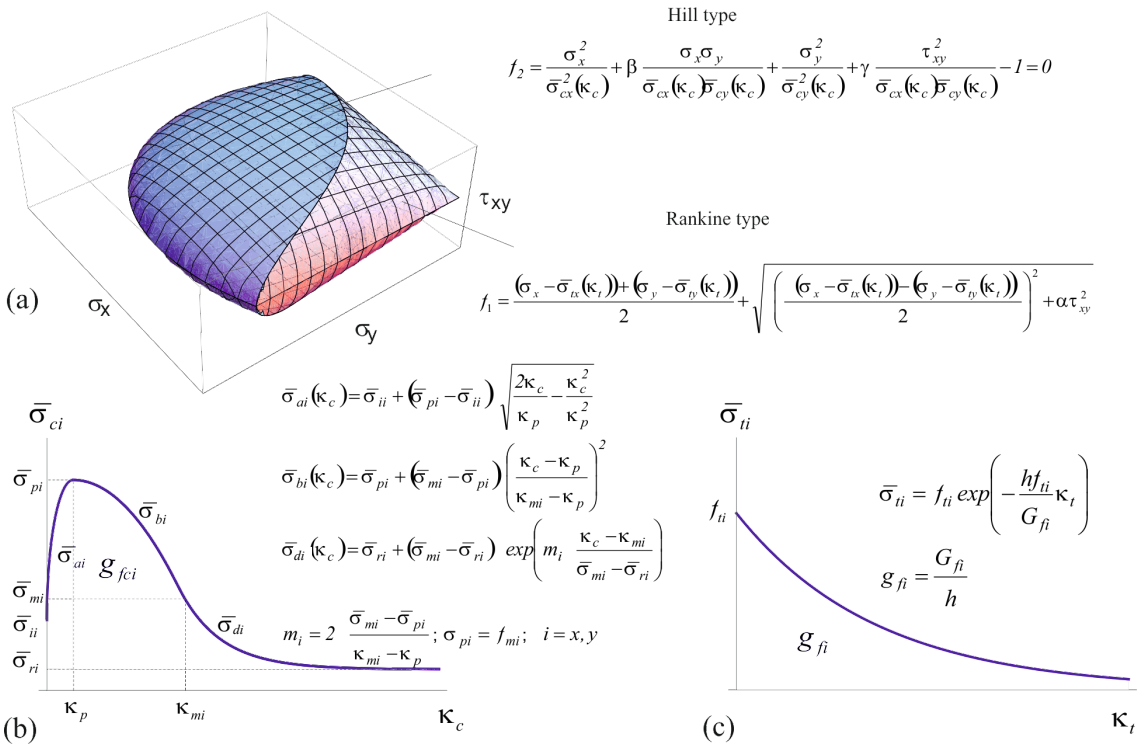

Figure 12. *(a) Biaxial strength envelope for masonry; stress-strain laws adopted for the material in (b) uniaxial compression and (c) uniaxial tension [32-34].*

If these experimental tests are performed under displacement control, they also provide the five required inelastic parameters, that is to say fracture energies in tension G_{fi} and compression G_{fci} in both directions x-y, as well as the plastic strain corresponding to the peak compressive strength, κ_p. The complete calibration of the model also requires additional non-standard tests [34] in order to determine the three remaining parameters α, β and γ (Figure 12a); in more detail, α weights the shear stress contribution to tensile failure, β controls the coupling between normal stress values in

519 case of compressive failure and γ weights the shear stress contribution to compressive
520 failure.

521 ***3.2 Calibration of the model for AAC masonry***

522 ***3.2.1 Biaxial failure envelope***

523 The parameters required for the construction of the failure envelope proposed by
524 Lourenço et al. have been derived on the basis of the results provided by the previously
525 described experimental tests on AAC masonry elements. The compressive strengths in
526 the two main directions *x*, *y* - respectively obtained as the average peak stress values σ_v
527 for PMC90 and PMC0 samples (see Table 1) - have been assumed equal to
528 $f_{mx} = f_{my} = 2.60$ MPa. The direct tensile strengths, respectively equal to $f_{tx} = 0.29$ MPa and
529 $f_{ty} = 0.24$ MPa, have been instead determined numerically, by simulating the three-point
530 bending tests carried out on samples BMF0 and BMF90 (Table 4), as better described in
531 Section 3.2.2.

532 The parameter α has been calculated through the least squares method, by
533 minimizing the function $\sum f_{1,j}^2(\alpha)$ with the non-linear optimization algorithm of
534 Levemberg-Marquard, being $f_{1,j}$ the plastic potential in the *j-th* experimental point (Figure
535 12a); in this way, the value of $\alpha = 0.5$ has been obtained. Similarly, the parameters β and
536 γ have been calculated by minimizing the function $\sum f_{2,j}^2(\beta,\gamma)$, so obtaining $\beta = -0.6$
537 and $\gamma = 5$.

538 The so calibrated failure envelope is depicted in Figure 13 in the $\sigma_x - \sigma_y$ plane,
539 through level curves corresponding to different values of the applied shear stress τ_{xy},
540 respectively equal to 0, 0.76, and 1.09 MPa. On the same graph, the corresponding

experimental values obtained from uniaxial and biaxial compression tests (Section 2.2), as well as from three-point bending (Section 2.3) and diagonal compression ones (Section 2.4), are also reported; as can be seen, the model error appears to be comparable with the experimental scattering. Furthermore, the obtained curves show that the behavior of AAC masonry is characterized by a weak anisotropy, with similar strength values in the two main directions *x*, *y*.

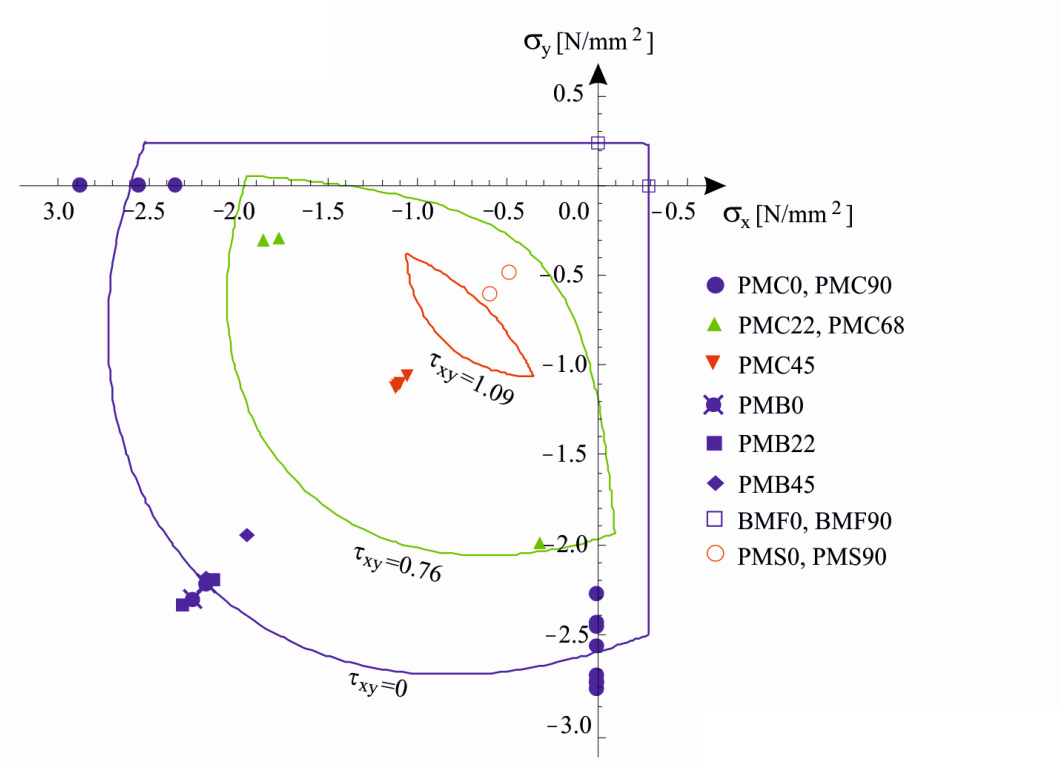

Figure 13. *Comparison between the adopted failure envelope [32-34] and the experimental results obtained for AAC masonry for different values of the applied shear stress* τ_{xy}.

3.2.2 Stress-strain laws in uniaxial compression and tension

Based on the experimental results, the plastic stress-strain laws for uniaxial compression in the two main directions − whose equations are reported for reading convenience in Figure 12b − have been calibrated by adopting the average values of compressive strengths ($f_{mx} = f_{my} = 2.60$ MPa), and elastic moduli ($E_x = 1700$ MPa,

555 E_y = 1400 MPa). The plastic strain corresponding to the peak compressive strength has
556 been assumed equal to κ_p = 0.3‰. The two fracture energies in compression have been
557 deduced numerically, through an inverse procedure based on the fitting of all the available
558 experimental data (Figure 14 a-b), so as to take into account the important scatter of the
559 softening branches. Since the experimental response was quite similar in the two main
560 directions (Figure 14c), also in this case a unique value of $g_{fcx} = g_{fcy} = 2.26 \cdot 10^{-3}$ N/mm^2
561 has been adopted. This value corresponds only to the local contribution of the $\overline{\sigma}_{ci} - \kappa_c$
562 diagram (where the subscript *i* refers to the material axis) and therefore the basis for its
563 definition is only numerical, in order to obtain objective results with respect to mesh
564 refinement [32].

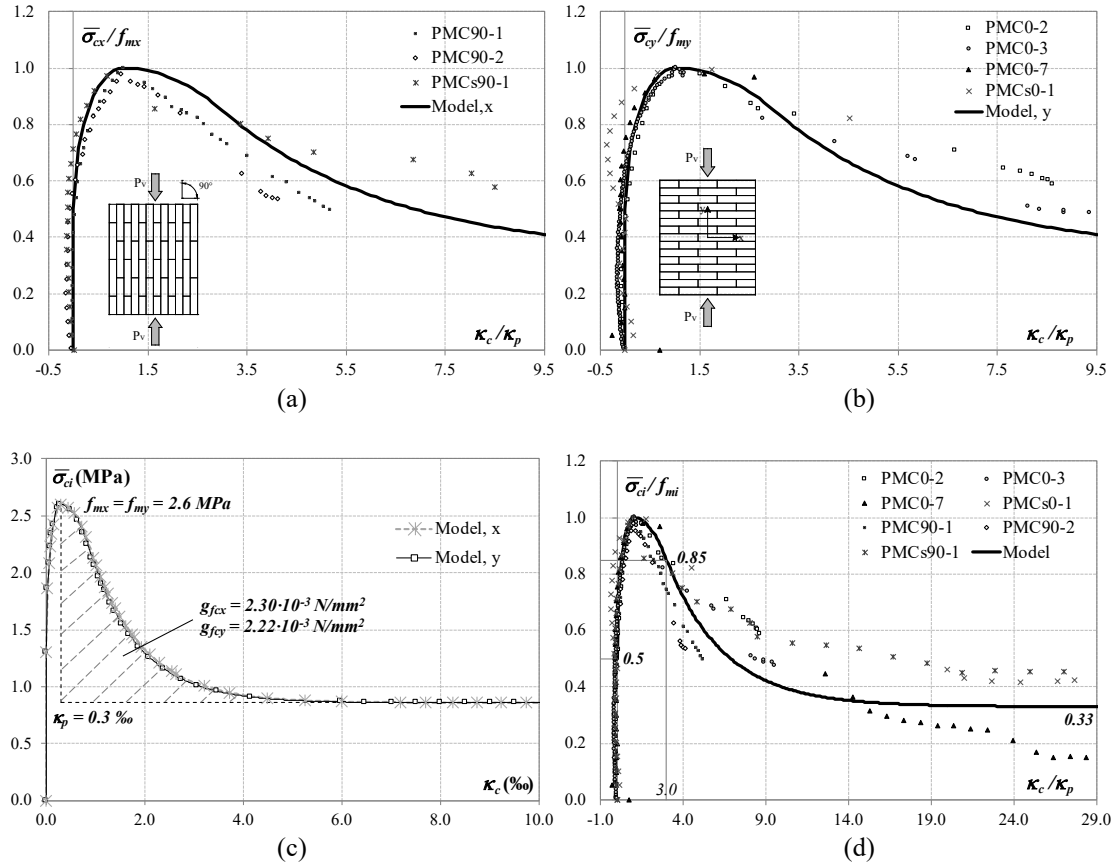

565
566
567
568

569 ***Figure 14.*** *Comparisons between the adopted inelastic law in compression for AAC masonry and the*
570 *available experimental data in (a) x and (b) y directions; (c) main parameters of the adopted laws in x*

571 *and y; (d) definition of a unique inelastic law and comparison with all the experimental results.*

572 The complete inelastic law adopted for compression in both the considered
573 directions, respectively parallel and perpendicular to bed joints, is reported in Figure 14d
574 in the dimensionless plane $\overline{\sigma}_{ci} / f_{mi}$ – κ_c / κ_p, where it is compared with the available
575 experimental data (specimens PMC0, PMCs0, PMC90, and PMCs90). On the same
576 Figure, the new parameters used herein for the definition of the shape of the curve are
577 also reported, that is to say $\overline{\sigma}_{ii} / f_{mi} = 0.5$, $\overline{\sigma}_{mi} / f_{mi} = 0.85$, $\overline{\sigma}_{ri} / f_{mi} = 0.33$, with reference
578 to the nomenclature adopted in Figure 12b and according to [32]. Moreover, with the
579 previous assumptions, parameter κ_{mi} becomes:

580 $$\kappa_{mi} = \frac{1080}{1627} \frac{G_{fci}}{h\, f_{mi}} + \kappa_p \,. \tag{3}$$

581 The stress-strain laws in uniaxial tension − whose equations are reported in
582 Figure 12c − have been instead calibrated by hypothesizing the same elastic moduli
583 obtained for compression and by adopting the average fracture energies determined
584 from three-point bending tests on BMF0 and BMF90 samples (respectively equal to
585 $G_{fx} = 7.10 \cdot 10^{-3}$ N/mm and $G_{fy} = 5.15 \cdot 10^{-3}$ N/mm, see Table 4). Direct tensile strengths
586 have been obtained from inverse analysis by using the general-purpose FE code
587 ABAQUS to simulate the above-mentioned three-point bending tests. To this scope,
588 each beam has been modeled by adopting a regular mesh formed by square 4-nodes
589 plane stress elements (CPS4 in the adopted FE code library), with 5 mm side, and this
590 discretization has been further refined in correspondence of the supports and of the
591 loading plate (Figure 15d). The problem of mesh dependence has been overcome by
592 scaling the fracture energies through the equivalent length $h = \sqrt{A_e}$, where A_e is the

593 area of the adopted element [33].

594 The interaction between the supports and the masonry sample has been taken into
595 account by introducing contact elements and by considering friction between AAC and
596 steel. The analyses have been performed by adopting quasi-static loading control to
597 overcome convergence problems, so obtaining the complete load-deflection curve. The
598 computed tensile strength average values in the two main masonry directions are
599 respectively equal to f_{tx} = 0.29 MPa and f_{ty} = 0.24 MPa.

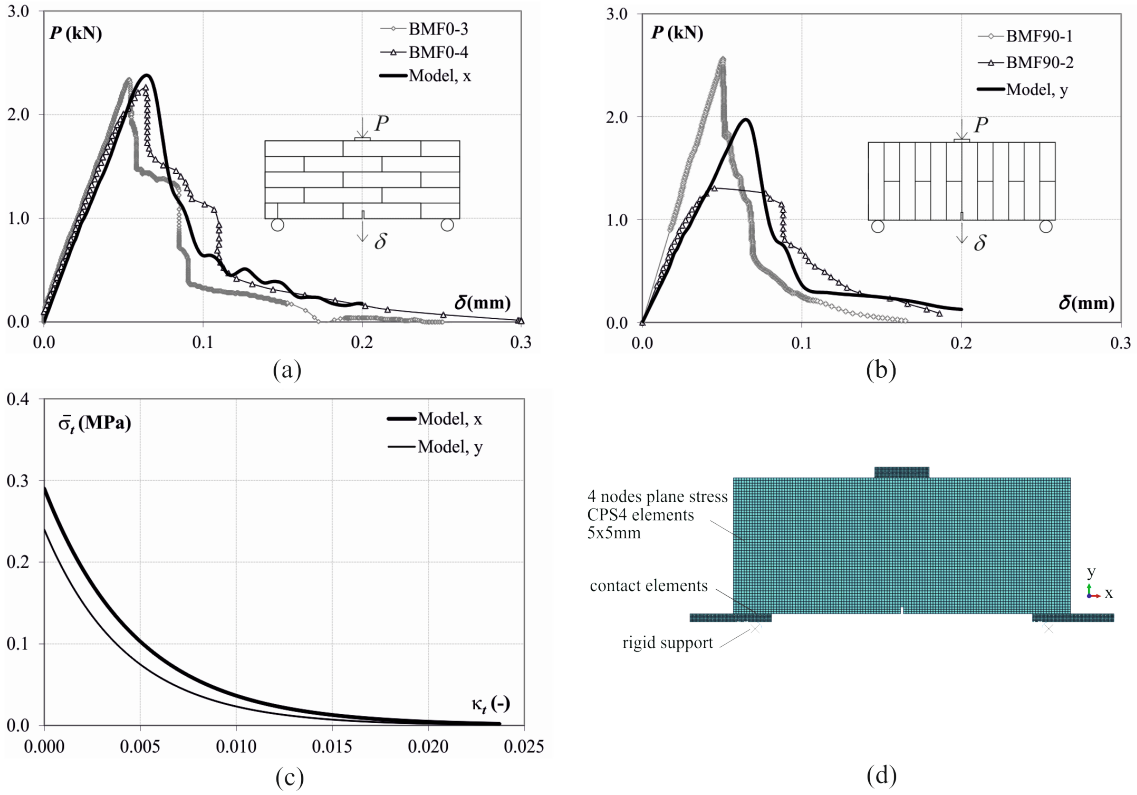

600

601 ***Figure 15.*** *Comparisons between numerical and experimental curves obtained for AAC masonry beams*
602 *(BMF) in terms of applied load P vs. midspan deflection δ in (a) x and (b) y directions. (c) Adopted*
603 *inelastic law in tension for AAC masonry in x and y directions; (d) FE mesh of AAC masonry beams.*

604 Figure 15a-b shows the comparison between numerical and experimental results
605 in terms of applied load P vs. midspan deflection δ, in case of BMF0 (Figure 15a) and
606 BMF90 samples (Figure 15b). As can be observed, in the first case (x direction)

607 experimental results are almost superimposed with each other and with the numerical
608 curve. On the contrary, experimental results relative to *y* direction present a larger
609 scatter, which is due to the different characteristics of the examined samples. As already
610 mentioned, specimen BF90-1 was indeed formed by an odd number of units, with the
611 notch placed at half-width of the central brick line, while specimen BMF90-2 was
612 realized with an even number of units, with the notch placed exactly in correspondence
613 of the glue joint. As regards numerical modeling, the geometry of specimen BMF90-2
614 has been considered, while the adopted mechanical properties have been set equal to the
615 average values deduced from tests, so obtaining an intermediate response.
616 Finally, Figure 15c reports the corresponding exponential softening plastic stress-
617 strain relations $\overline{\sigma}_{ti}-\kappa_t$ in *x* and *y* directions.

618

619 **4. SIMULATION OF THE BEHAVIOR OF A FULL-SCALE AAC MASONRY**
620 **WALL**

621 The effectiveness of the so calibrated plastic model and its ability of correctly
622 describe the behavior of AAC masonry structures has been subsequently verified
623 through the simulation of an experimental test carried out at the University of Pavia on a
624 full-scale AAC masonry wall subjected to a vertical load and an increasing in-plane
625 horizontal force [31]. The geometry and the adopted test arrangement are schematized
626 in Figure 16a. As can be seen, the considered wall was 1.5 m long, 2.75 m high and
627 0.3 m wide, and it was assembled by using 625 × 300 × 250 mm AAC blocks, which are
628 bigger than those used to calibrate the adopted constitutive model. The specimen was
629 built with thin mortar layers (2-3 mm thick) and filled head joints. Reinforced concrete

beams – whose dimensions can be found in [31] − were built at the top of the wall, to guarantee a better load distribution, and at the bottom, acting as a foundation. The chosen test setup was indeed a cantilever system (fixed at the base and free at the top) with a constant vertical load of 200 kN applied on the top beam through hydraulic jacks. The horizontal load was instead applied through a displacement-controlled horizontal hydraulic actuator, performing three fully reversed cycles for the chosen target displacement level, until the reaching of a horizontal displacement equal to 0.6% of the wall height [31].

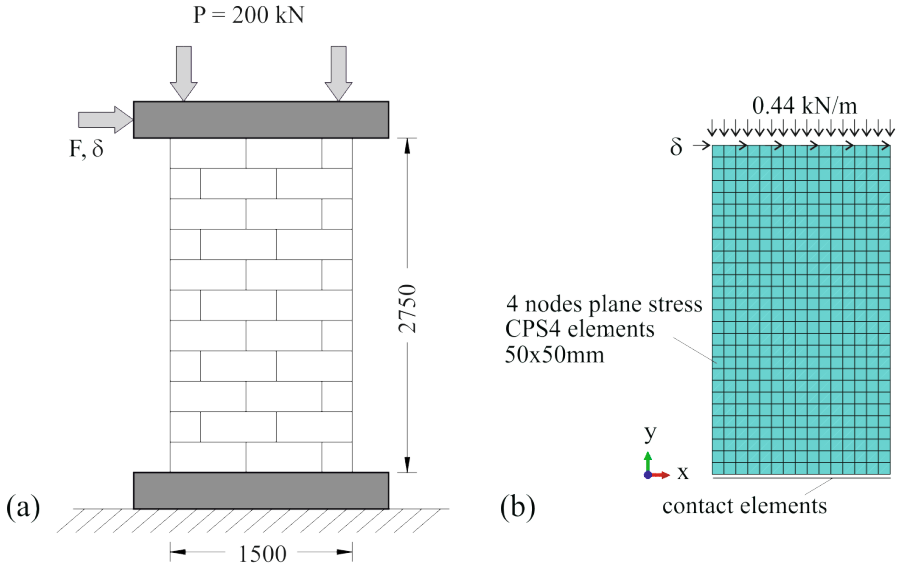

Figure 16. *Tests on a full scale AAC masonry wall: (a) sketch of the experimental setup [31]; (b) adopted FE mesh.*

The considered wall has been modeled by adopting a uniform mesh, formed by square 4-node plane stress elements (CPS4) with 50 mm side, as shown in Figure 16b. For sake of simplicity, the two reinforced concrete beams have not been included in the FE model, by simply introducing contact elements at the base and considering friction between the AAC wall and the support. The horizontal force has been replaced by a uniform distribution of prescribed displacements δ. The mechanical behavior of AAC

masonry has been simulated through the constitutive model described in the previous Section. Since the mechanical properties of AAC blocks used for the realization of the examined wall were not exactly the same of those determined in the experimental program illustrated herein, both the compressive strengths as well as the elastic moduli were properly updated, according to the corresponding values reported in [31]. In more detail, the following values have been assumed: f_{mx} = 1.90 MPa, f_{my} = 2.20 MPa, $E_x = E_y$ = 1498 MPa. On the contrary, for the other required elastic and inelastic properties – which were not available in [31] - the values determined in Section 3 have been assumed. This modeling choice seems to be reasonable, since the adopted model is based on an orthotropic formulation and also its calibration to the case of AAC masonry is based on weakly anisotropic data (e.g. the elastic moduli in the two principal directions are different). As a consequence, the adoption of slightly different strength values in the two principal direction (which are anyway comparable with those adopted in Section 3), should not alter the effectiveness of the proposed approach.

The NLFE analysis has been carried out under displacement control, by simply modeling the last loading cycle. Also in this case, a quasi–static analysis has been performed to mitigate convergence problems, and the controlled displacement has been increased monotonically up to failure. The so obtained results have been reported in terms of applied load F vs. top horizontal displacement δ in Figure 17, where they are compared with the experimental response. The latter represents the envelope curve of the three fully reversed cycles performed during the test. As can be observed, the model is able to describe with sufficient accuracy the behavior of the examined full-scale wall until the reaching of the ultimate load, whose value is also predicted.

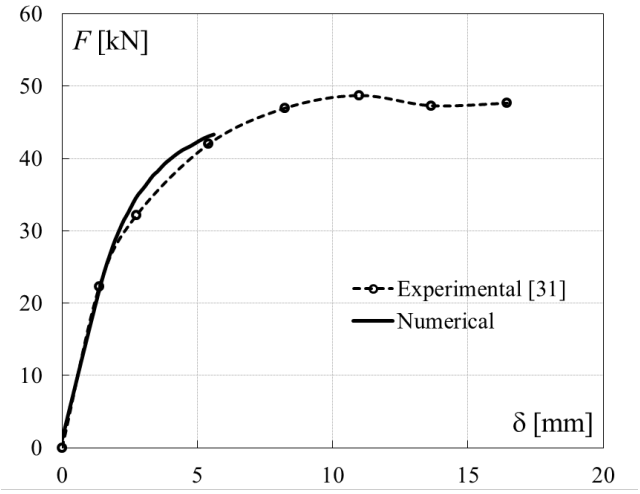

Figure 17. *Comparison between numerical and experimental results in terms of applied load F vs. horizontal displacement δ.*

Anyhow, it should be underlined that the numerical response appears to be significantly less ductile than the experimental one. The underestimated ductility is due to important convergence problems that have been reported also in other works that adopt the same algorithm [43, 44]. In particular, van der Meer [44] analyzed the reasons of the convergence weakness of the subroutine (apex, return-mapping, multi-surface plasticity algorithm) and proposed some promising improvements that are, however, out of the scope of this work.

5. CONCLUSIONS

The present work illustrates the main results of an experimental program focused on the mechanical characterization of AAC masonry. To this aim, the following test typologies have been performed:

– uniaxial compression tests on masonry panels under force/displacement control;

– biaxial compression tests on masonry panels;

– diagonal compression tests on small masonry panels;
– three-point bending tests on masonry beams under force/CMOD control.

The results have been used to calibrate a well-known macroscopic anisotropic constitutive model already developed for ordinary masonry and available in the technical literature [32-34]. This model has been subsequently applied to simulate numerically the behavior of a full-scale AAC masonry wall subjected to a pushover test [31].

The main conclusions of this research are summarized herein:

– if properly calibrated, numerical anisotropic models proposed for traditional masonry can be also used for AAC masonry;
– AAC masonry is characterized by a very weak anisotropy due to the particular cementitious glue adopted for the realization of thin joints;
– observed failure modes reveal that if joints are correctly realized by skilled labor, they do not represent a significant weakness in masonry behavior.

For these reasons, as a first approximation, the mechanical properties of the raw AAC material (with a similar density and moisture content) can be used for mechanical models and finite element simulations on masonry elements.

ACKNOWLEDGEMENTS

Mr. Matteo Riva is gratefully acknowledged for his contribution in the execution of experimental tests. The authors would also like sincerely to thank Prof. Ivo Iori and M.Sc. Eng. Giuseppe Gazzola for their interest and scientific support in this research.

REFERENCES

[1] Narayanan N, Ramamurthy K. Structure and properties of aerated concrete: a review. Cem Concr Compos 2000; 22: 321-329.

[2] Laukaitis A, Fiks B. Acoustical properties of aerated autoclaved concrete. Appl Acoust 2006; 67: 284-296.

[3] Limbachiya MC, Roberts JJ Eds. Proc. 4th Int Conf on AAC - Autoclaved Aerated Concrete: innovation and development. Taylor & Francis, London, 2005.

[4] Wittmann FH Eds. Proc. 3rd RILEM Int Symp on AAC - Advances in Autoclaved Aerated Concrete. Balkema, Rotterdam, 1992.

[5] Aroni S, De Groot GJ, Robinson MJ, Svanholm G, Wittmann FH Eds. Autoclaved aerated concrete: properties, testing and design. RILEM Recommended Practice, London: E&FN Spon, 1993.

[6] Marzahn GA. Extended investigation of mechanical properties of masonry units. LACER 2002; 7: 237-254.

[7] Muszynski LC, Gulas S. Fire resistance and performance of alternative concrete wall systems. J Constr Edu 2001; 6: 146-154.

[8] Delmotte P, Rivillon P, Wesierski V, Hurez M. Study on shear walls realized with autoclaved aerated concrete masonry (in French). Cahier du CSTB n. 3492, Livraison 445, 2003.

[9] Klingner RE, Tanner JE, Varela JL, Barnett RE. Autoclaved aerated concrete: innovative materials and civil infrastructure. Proc. Int Work on Innovation in Materials and Design of Civil Infrastructure, Cairo, 2005: 1-36.

[10] Tanner JE, Varela JL, Klingner RE, Brightman MJ, Cancino U. Seismic testing of autoclaved aerated concrete shearwalls: a comprehensive review. ACI Struct J 2005;

734 102(3): 374-382.
735 [11] Wittmann FH Eds. Autoclaved Aerated Concrete, Moisture and Properties. Elsevier,
736 Amsterdam, 1983.
737 [12] Lourenço PB. Experimental and numerical issues in the modelling of the mechanical
738 behavior of masonry. In Roca P et al Eds: Structural Analysis of Historical
739 Constructions II. Barcelona: CIMNE, 1998, pp. 57-91.
740 [13] Johnson FB, Thompson JN. Development of diametric testing procedures to provide
741 a measure of strength characteristics of masonry assemblages. In Johnson FH Ed:
742 Designing, Engineering and Constructing with Masonry Products, Gulf Publishing,
743 Houston, 1969, pp. 51-57.
744 [14] Drysdale RG, Hamid AA. Behavior of concrete block masonry under axial
745 compression. Amer Concr Inst J 1979; 76(6): 707-721.
746 [15] Hamid AA, Drysdale RG. Proposed failure criteria for concrete block masonry under
747 biaxial stresses. ASCE J Struct Div 1981; 107(8): 1675-1687.
748 [16] Samarasinghe W, Hendry AW. The strength of brickwork under biaxial tension-
749 compression. In: Proc 7th Int Symp on Load Bearing Brickwork, London, 1980, pp.
750 129-140.
751 [17] Page AW. The biaxial compressive strength of brick masonry. Proc Instn Civ Engrs
752 1981; 71(2): 893-906.
753 [18] Page AW. The strength of brick masonry under biaxial compression-tension. Int J
754 Masonry Constr 1983; 3(1): 26-31.
755 [19] Dhanasekar M, Page AW, Kleeman PW. The failure of brick masonry under biaxial
756 stresses. Proc Instn Civ Engrs 1985; 79(2): 295-313.
757 [20] Dhanasekar M, Kleeman PW, Page AW. Biaxial stress-strain relations for brick

masonry. ASCE J Struct Eng 1985; 111(5): 1085-1100.

[21] Hegemier GA, Nunn RO, Arya SK. Behavior of concrete masonry under biaxial stresses. Proc North Amer Masonry Conf, Univeristy of Colorado, Boulder, 1978, pp. 1.1-1.28.

[22] Mojsilović N. Strength of masonry subjected to in-plane loading: A contribution. Int J Solid Struct 2011; 48: 865-873.

[23] Badarloo B, Tasnimi AA, Mohammadi MS. Failure criteria of unreinforced grouted brick masonry based on a biaxial compression test. Scientia Iranica Civ Eng 2009; 16(6): 502-511.

[24] da Porto F. In Plane Cyclic Behaviour of Thin Layer Joint Masonry. PhD Thesis, University of Trento, Italy, 2005.

[25] Dhanasekar M, da Porto F. Review of the progress in thin bed technology for masonry construction. In: 11th Canadian Masonry Symposium, Toronto, Ontario, 2009, pp. 1003-1014.

[26] Fried AN, Marrocchino E, Bradsell C, Roberts JJ. Unreinforced Solid Dense Concrete Block Walls Constructed Using Thin Bed Technology, Structural Engineer UK, 2005, 83(12): 33-37.

[27] Thamboo J A, Dhanasekar M, Yan C. Characterisation of flexural bond strength in thin bed concrete masonry.In: 15th Int Brick and Block Masonry Conf. Federal University of Sao Carlos and Federal University of Santa Catarina, 2012.

[28] Vermeltfoort A. Shear, Bond and 2D Compressive Properties of Thin Bed Mortar Masonry. In: Proc. 13th Int Brick and Block Masonry Conf, Amsterdam, 2004, pp. 1-10.

[29] Tanner JE, Varela JL, Klingner RE, Fouad FH, Barnett RE. Technical basis for US

782 design provisions for Autoclaved Aerated Concrete masonry. In Limbachiya et al. Eds:
783 Autoclaved Aerated Concrete, Innovation and Development, Taylor & Francis,
784 London, 2005, pp. 325-336.
785 [30] Shermer D. Seismic behavior of Autoclaved Aerated Concrete masonry
786 constructions. In Limbachiya et al. Eds: Autoclaved Aerated Concrete, Innovation and
787 Development, Taylor & Francis, London, 2005, pp. 387-394.
788 [31] Costa AA, Penna A, Magenes G. Seismic Performance of Autoclaved Aerated
789 Concrete (AAC) Masonry: From Experimental Testing of the In-Plane Capacity of
790 Walls to Building Response Simulation. J Earthquake Eng 2011; 15(1): 1-31.
791 [32] Lourenço PB. Computational strategies for masonry structures. Ph.D. Thesis, TU
792 Delft, The Netherlands, 1996.
793 [33] Lourenço PB, De Borst R, Rots JG. A plane stress softening plasticity model for
794 orthotropic materials. Int J Numer Meth Eng 1997; 40: 4033-4057.
795 [34] Lourenço PB, Rots JG, Blaauwendraad A. Continuum model for masonry parameter
796 estimation and validation. ASCE J Struct Eng 1998; 124(6): 642-652.
797 [35] Ferretti D, Michelini E, Rosati G. Cracking in autoclaved aerated concrete:
798 Experimental investigation and XFEM modeling. Cem Concr Res 2015; 67: 156-167.
799 doi: 10.1016/j.cemconres.2014.09.005.
800 [36] Ferretti D, Gazzola G, Iori I, Michelini E, Rosati G. Calibration of a nonlinear
801 anisotropic mechanical model for AAC masonry (in Italian). Proc. 18th C.T.E.
802 Congress, Brescia, 2010, pp.153-162.
803 [37] Wittmann FH, Gheorghita I. Fracture toughness of autoclaved aerated concrete. Cem
804 Concr Res 1984; 14: 369-374.
805 [38] Trunk B, Schober G, Helbling AK, Wittmann FH. Fracture mechanics parameters of

806 autoclaved aerated concrete. Cem Concr Res 1999; 29: 855-859.
807 [39] UNI EN 1996-1-1:2006. Eurocode 6 - Design of masonry structures - Part 1-1:
808 General rules for reinforced and unreinforced masonry structures.
809 [40] Tanner JE. Design provisions for autoclaved aerated concrete (AAC) structural
810 systems. PhD Thesis, University of Texas, Austin, 2003.
811 [41] Lourenço PB, Palácio K, Prieto F. Implementation of a constitutive model for
812 masonry shells as a stand-alone subroutine. Report 02-DEC/E-13, Universidade do
813 Minho, Departamento de Engenharia Civil, 2002.
814 [42] ABAQUS 6.12. Online Documentation. Dassault Systémes Simulia Corp.
815 [43] Dhanasekar M, Haider W. Explicit finite element analysis of lightly reinforced
816 masonry shear walls. Comp & Struct 2008; 86(1), 15-26.
817 [44] van der Meer LJ, Unbonded post-tensioned shear walls of calcium silicate element
818 masonry, PhD Thesis, Eindhoven University of Technology, 2013, ISBN: 978-90-386-
819 3374-9.
820

LIST OF FIGURES

obtained for AAC masonry for different values of the applied shear stress τ_{xy}.

Figure 14. *Comparisons between the adopted inelastic law in compression for AAC masonry and the available experimental data in (a) x and (b) y directions; (c) main parameters of the adopted laws in x and y; (d) definition of a unique inelastic law and comparison with all the experimental results.*

Figure 15. *Comparisons between numerical and experimental curves obtained for AAC masonry beams (BMF) in terms of applied load P vs. midspan deflection δ in (a) x and (b) y directions. (c) Adopted inelastic law in tension for AAC masonry in x and y directions; (d) FE mesh of AAC masonry beams.*

Figure 16. *Tests on a full scale AAC masonry wall: (a) sketch of the experimental setup [31]; (b) adopted FE mesh.*

Figure 17. *Comparison between numerical and experimental results in terms of applied load F vs. horizontal displacement δ.*

LIST OF TABLES

Table 1. *Uniaxial compression tests on AAC masonry panels (PMC and PMCs): effective dimensions of the specimens and experimental failure loads.*

Table 2. *Uniaxial compression tests on AAC masonry panels (PMC and PMCs): elastic moduli E_x, E_y, Poisson ratio ν and compressive peak strains ε_{px} and ε_{py}.*

Table 3. *Biaxial compression tests on AAC masonry panels (PMB): effective dimensions of the specimens and experimental failure loads.*

Table 4. *Three-point bending tests on AAC masonry beams (BMF): effective dimensions of the specimens, experimental failure loads, indirect tensile strengths and fracture energies in tension.*

Table 5. *Diagonal compression tests on small AAC masonry panels (PMS): effective dimensions of the specimens and experimental failure loads.*